Nanoscale Horizons

The home for rapid reports of exceptional significance in nanoscience and nanotechnology

rsc.li/nanoscale-horizons

ROYAL SOCIETY
OF CHEMISTRY | Celebrating IYPT 2019

COMMUNICATION
Xuezhi Zheng, Ventsislav K. Valev *et al.*
Measuring optical activity in the far-field from a racemic nanomaterial: diffraction spectroscopy from plasmonic nanogratings

NCNST

Check for updates

Measuring optical activity in the far-field from a racemic nanomaterial: diffraction spectroscopy from plasmonic nanogratings†

Christian Kuppe, [ID] [a] Xuezhi Zheng,*[b] Calum Williams,[c] Alexander W. A. Murphy,[a] Joel T. Collins,[a] Sergey N. Gordeev,[d] Guy A. E. Vandenbosch[b] and Ventsislav K. Valev [ID] *[ad]

Recent progress in nanofabrication has redrawn the boundaries of the applicability of chiroptical (chiral optical) effects. Chirality, often expressed as a twist in biomolecules, is crucial for pharmaceuticals, where it can result in extremely different chemical properties. Because chiroptical effects are typically very weak in molecules, plasmonic nanomaterials are often proposed as a promising platform to significantly enhance these effects. Unfortunately, the ideal plasmonic nanomaterial has conflicting requirements: its chirality should enhance that of the chiral molecules and yet it should have no chiroptical response on its own. Here, we propose a unique reconciliation to satisfy the requirements: a racemic plasmonic nanomaterial, consisting of equal amounts of opposite chiral unit cells. We show how diffraction spectroscopy can be used to unveil the presence of chirality in such racemic nanogratings in the far-field. Our experiments are supported by numerical simulations and yield a circular intensity difference of up to 15%. The physical origin is demonstrated by full wave simulations in combination with a Green's function – group-theory-based analysis. Contributions from Circular Dichroism in the Angular Distribution of Photoelectrons (CDAD) and pseudo/extrinsic chirality are ruled out. Our findings enable the far-field measurement and tuning of racemic nanomaterials, which is crucial for hyper-sensitive chiral molecular characterization.

New concepts

Chiral plasmonic nanomaterials have revolutionized chirality, with new theoretical parameters that enable superchiral light and negative refractive index materials. There are many potential applications, such as ultra-thin-film optical components, nanorobotics, and especially enhanced optical processes with chiral molecules. In order for the chiral nanostructures to enhance the optical activity in molecules without affecting it themselves, the nanostructures need to be in a racemic mixture, *i.e.* a 50:50 ratio of enantiomorphs, with zero net optical activity. Yet, the chirality of these same nanostructures needs to be tailored to that of the chiral molecules. Which leads to a contradiction: how to tailor the optical activity in a material with zero optical activity? Our answer appears from looking at the question from a new direction. We show that diffraction spectroscopy can be used to unveil the presence of chirality, in such racemic nanomaterials, even in the far-field. We show very large values for the optical activity in diffracted beams and we provide a rigorous theoretical and conceptual support for our findings. This work creates opportunities to explore and tailor the interactions between plasmonic nanoparticles and chiral molecules: it removes an important roadblock for the entire research field.

Introduction

Recently, the field of chirality has experienced a paradigm shift, driven by experimental progress in nanofabrication[1,2] and by theoretical insights into the chirality parameters.[3–6] These parameters include geometric and optical chirality that both lead to fascinating physical properties, such as negative refractive index[7,8] and superchiral light states.[9,10] In turn, these concepts are enabling applications, including super-lenses and hyper-sensitive molecular characterization.[10]

Molecular chirality is ubiquitous in bio-organisms and, hence, a crucial topic for pharmacology.[11,12] Indeed, the mirror images (or enantiomers) of many bio-molecules can have very distinct functions.[13] However, molecular synthesis usually yields an equal proportion of both enantiomers (or a racemic mixture).[14] Additional chemical processes are therefore required to separate the enantiomers and at each step their ratio needs to be measured.[2,15]

Since the very discovery of molecular chirality, optical activity (OA) has been used to measure the ratio of enantiomers (or enantiomeric excess). OA results from the difference in interaction between enantiomers with left- or right-hand circularly polarized light (CPL). Although OA is widely used in chemistry, the effect is typically very weak; this is because the chiral pitch of CPL is orders of magnitude larger than the chiral pitch in molecules.[13]

[a] *Centre for Photonics and Photonic Materials and Centre for Nanoscience and Nanotechnology, University of Bath, Bath, BA2 7AY, UK. E-mail: v.k.valev@bath.ac.uk*
[b] *Department of Electrical Engineering (ESAT-TELEMIC), KU Leuven, Kasteelpark Arenberg 10, BUS 2444, Heverlee, 3001, Belgium. E-mail: xuezhi.zheng@esat.kuleuven.be*
[c] *Electrical Engineering Division, Department of Engineering, University of Cambridge, 9 JJ Thomson Avenue, Cambridge, CB3 0FA, UK*
[d] *Centre for Nanoscience and Nanotechnology, University of Bath, Bath, BA2 7AY, UK*
† Electronic supplementary information (ESI) available. See DOI: 10.1039/c9nh00067d

Metal nanostructures bridge this gap. These nanostructures benefit from surface plasmon resonances; whereby coherent oscillations of the surface electrons can be excited by visible light.[16] These oscillations occur at the same frequency, but with a much shorter wavelength, which effectively confines light at the nanoscale and therefore enhances the interaction with molecules.[17–19] As a consequence, chiral plasmonic nanomaterials exhibit pronounced chiral optical (chiroptical) effects, which can unfortunately overshadow the molecular response.[20–24]

Although achiral plasmonic nanoparticles have been demonstrated to successfully enhance the chiroptical response of some molecules, such as cysteine and riboflavin,[20,25] this enhancement is not optimal, as it does not benefit from the chirality of the plasmonic fields. By contrast, a racemic mixture of chiral plasmonic nanostructures has no net OA, but strong local chirality in the plasmonic near-field that chiral molecules can couple to. The response from such racemic nanomaterials can be highly sensitive to the enantiomeric excess of molecules.[26] However, the lack of chiroptical response in the far-field makes it difficult to tailor the material to molecules.[27–29]

Here, we demonstrate for the first time a detection scheme that allows the measurement of the chiroptical response of a racemic nanograting in the far-field. We show that racemic nanogratings can yield extremely large chiroptical responses of up to 15%, comparable to previously reported OA for chiral nanogratings.[23,30–33] Previous work has focused on circular intensity difference spectroscopy from individual diffraction beams.[23,30–34] Here, we present a comprehensive analysis of up to four orders of diffraction and the physical origin of the measured far-field response is exploited by full-wave electromagnetic simulations. The measured far-field response is studied in the framework of a Green's function – group-theory-based approach. We discuss and rule out contributions from false chirality, such as the Circular Dichroism in the Angular Distribution of Photoelectrons (CDAD) or pseudo/extrinsic chirality.

Results

In Fig. 1a, left- and right-circularly polarized (LCP and RCP) light is used to illuminate gold nanogratings. The spatial period of the nanogratings was chosen to produce multiple diffraction order beams in the visible spectrum. Those diffracted beams are analyzed using circular intensity difference (CID) spectroscopy. The gold nanogratings studied in this work were fabricated using electron beam lithography on a silicon-silicon dioxide wafer (dioxide layer thickness of 300 nm). The gold layer (30 nm thickness) was stabilized using a chromium adhesion layer (3 nm thick). The thickness profile is presented schematically in Fig. 1b and the fabrication details are given in the Methods section. The period of the gratings was 2.4 μm. Each square unit cell consists of a 2 × 2 arrangement of gold elements and each element is 1 μm large. The nanowire width, and the nearest neighbor separation is 200 nm. Furthermore, each element is rotated by 90° with respect to its neighbor. The individual nanoelements assemble into three different chiral
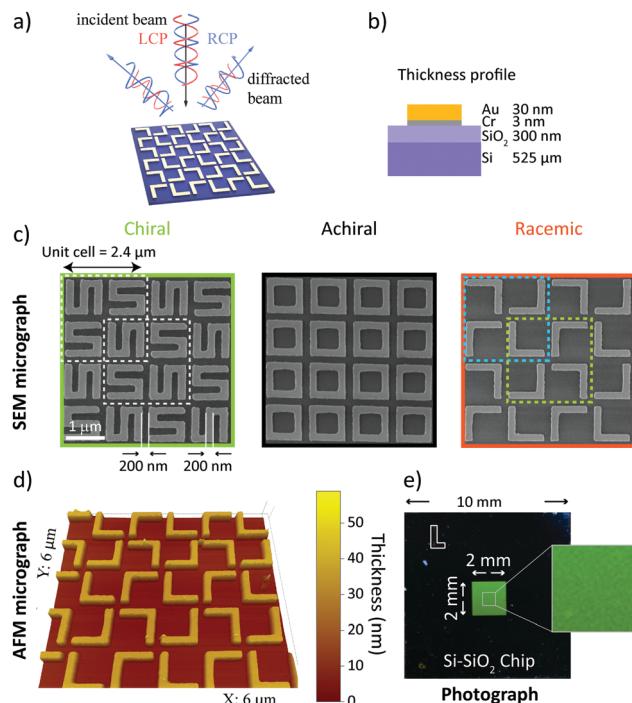

Fig. 1 Nanomaterials can be chiral, achiral or racemic; here S-shaped, square-rings, and L-shaped, respectively. In (a), the concept of circular intensity difference spectroscopy for individual diffraction order beams is presented schematically. Left- and right circularly polarized light beams (red and blue spirals, respectively) are normally incident on a gold nanograting. The resulting diffraction orders are subsequently probed for differences in their intensity. The thickness profile of the nanogratings is shown in (b). The central panel (c), shows the scanning electron microscopy (SEM) micrographs of the resulting samples. The S-shaped chiral sample is shown in the green box. A unit cell consists of a 2 × 2 element matrix, where each element is rotated by 90° relative to its neighbor. The unit cell size is 2.4 μm and each element is 1 μm long, with an arm width of 200 nm and spacing of 200 nm. The achiral chip design (black box) is made of square-rings and the racemic chip (orange box) consists of L-shaped structures – the dimensions are the same as for the chiral nanograting. The cyan and green dashed lines in the racemic case indicate the two enantiomeric unit cells. In (d), the results of a topological study of the racemic nanograting via atomic force microscopy (AFM) are presented and its homogeneity over a large area (4 mm²) is shown with a photograph in (e).

states – chiral (S-shaped), achiral (square-rings) and racemic (L-shaped). The different gratings were characterized with scanning electron microscopy (SEM) and are shown in Fig. 1c. The L-shaped nanostructures naturally result in unit cells with opposite handedness (highlighted with cyan and yellow dashed lines, in Fig. 1c) and are therefore macroscopically racemic. The racemic nanogratings were further characterized via atomic force microscopy (AFM) and the associated micrograph is presented in Fig. 1d. On a larger scale, the good homogeneity of the total nanograting array (area 4 mm²) is demonstrated by the uniformity of the nanostructured area in the photograph image shown in Fig. 1e.

The apparatus used to study the nanogratings is shown schematically in Fig. 2a, with a detailed description in the Methods section. A supercontinuum light source was used to generate coherent white light, with a linear polarizer and an
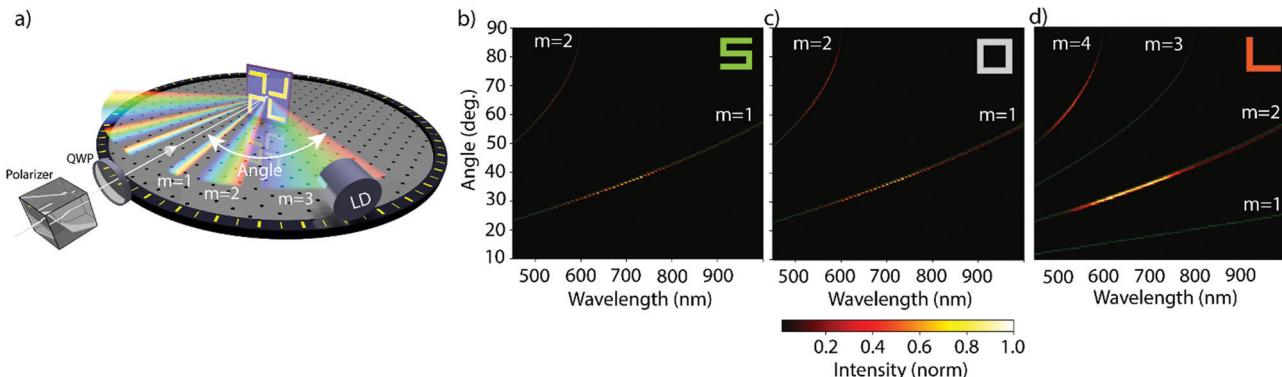
Fig. 2 Our nanogratings of chiral, achiral and racemic nanomaterials exhibit multiple diffraction beams in the visible part of the spectrum. The apparatus used to study the circular intensity difference (CID) in diffraction, and intensity pattern for each nanograting, is schematically shown in (a). The polarization state of the incident coherent white light was controlled by a linear polarizer and a quarter-waveplate (QWP), the beam was directed at normal incidence with respect to the nanograting. The diffraction pattern in reflection was measured in the horizontal plane using a fiber-based light detection (LD) system rotated around the sample. Since the nanogratings exhibit C_4 symmetry only the positive diffraction orders between 10–90° were measured. The resulting intensities for left circularly polarized (LCP) light are shown on the bottom. The intensities for the samples, shown in Fig. 1c, are represented by normalized heatmaps with the wavelength on the x- and the diffraction angle on the y-axis. The green lines show the predicted position of the diffracted order beams for periods of 1.2 μm (for S- and square-ring shaped samples) and 2.4 μm (for L-shaped samples) are given and agree with the experimental results.

achromatic waveplate to control its polarization state. Since all our nanogratings exhibit C_4 symmetry (unchanged when rotated by 90° about its normal axis), the investigation was limited to the in-plane horizontal diffraction orders. Because these diffracted beams are the same on both sides of the incident beam, we focused our attention on the positive diffracted order beams ($m = 1, 2$, *etc.*), as indicated in Fig. 2a. The diffracted light was measured with a light detection (LD) scheme, consisting of a microscope objective and an optical fiber connected to a spectrometer for analysis. For the individual nanogratings, the resulting diffraction patterns are shown in Fig. 2b–d; presented as intensity heatmaps. The spatial distribution of the diffracted beams is in good agreement with the predicted spatial distribution from the grating equation (green lines).[34] The effective period of the S-shaped and square-ring nanogratings is halved to 1.2 μm as a consequence of the unit cell design shown in Fig. 1c. While the normalized intensity for the L-shaped gratings produces four distinct diffraction orders ($m = 1$ to 4), the first and third order beams are approximately 50 times less intense than the second and fourth order beams; barely visible in the intensity heatmaps.

The optical activity of the nanogratings was determined by measuring the CID in each diffraction order beam. CID is defined as

$$\mathrm{CID} = \frac{I_{\mathrm{RCP}} - I_{\mathrm{LCP}}}{I_{\mathrm{RCP}} + I_{\mathrm{LCP}}}, \qquad (1)$$

with I_{RCP} and I_{LCP} representing the measured intensities for RCP and LCP illumination, respectively.

Additionally, to corroborate the experimental results and further explain the physical origins of the observed effects, finite difference simulations were carried out using Lumerical[35] (detailed description in the Methods section). The measured and simulated far-field response of the nanogratings are presented in Fig. 3. The results from the experimental and numerical analysis

are in excellent agreement for both the spatial distribution and the CID response for each nanograting. The chiral S-shaped nanogratings (Fig. 3a) exhibit a large CID of up to 20% and a change of sign between the first and second diffracted order beams. For the associated mirrored S-shaped nanogratings, the response is opposite in sign, as expected from chirality (see Fig. S1, ESI†). The results are in good agreement with the numerical simulations.

The achiral square-ring-shaped nanogratings (Fig. 3b) should exhibit no CID and therefore, the measured response indicates the noise level in both the experiments and the numerical simulations. Experimentally, the maximum CID is just below 5%, which is significantly lower than the response obtained for the chiral nanogratings. For the simulations, the numerical noise level is as low as 10^{-7}. Sources for the experimental error are thought to be fabrication imperfections, detection uncertainties and small differences in the fiber coupling efficiency.

Unlike the achiral nanogratings, the racemic L-shaped nanogratings, do exhibit CID. Our experimental results (Fig. 3c) demonstrate a large response of up to 15%, comparable to the S-shaped nanogratings with up to 20%. This counter-intuitive result is in good agreement with the numerical simulations, especially the strong responses in the first and third order diffracted beams. A slight spectral shift (red-shift) between the experimental and numerical results can be observed, due to the difference between the nominal sample geometry (ideally realized in a simulation) and the nanofabricated samples, prone to defects, see AFM micrograph in Fig. 1d. The robustness of the far-field response from the racemic L-shaped nanogratings was further investigated by measuring the effect of sample rotation with respect to the input beam. This investigation shows no significant net-effect on the observed results (see Fig. S2, ESI†).

In order to explain the CID effects from the racemic L-shaped nanostructures, a near-field to far-field transformation procedure
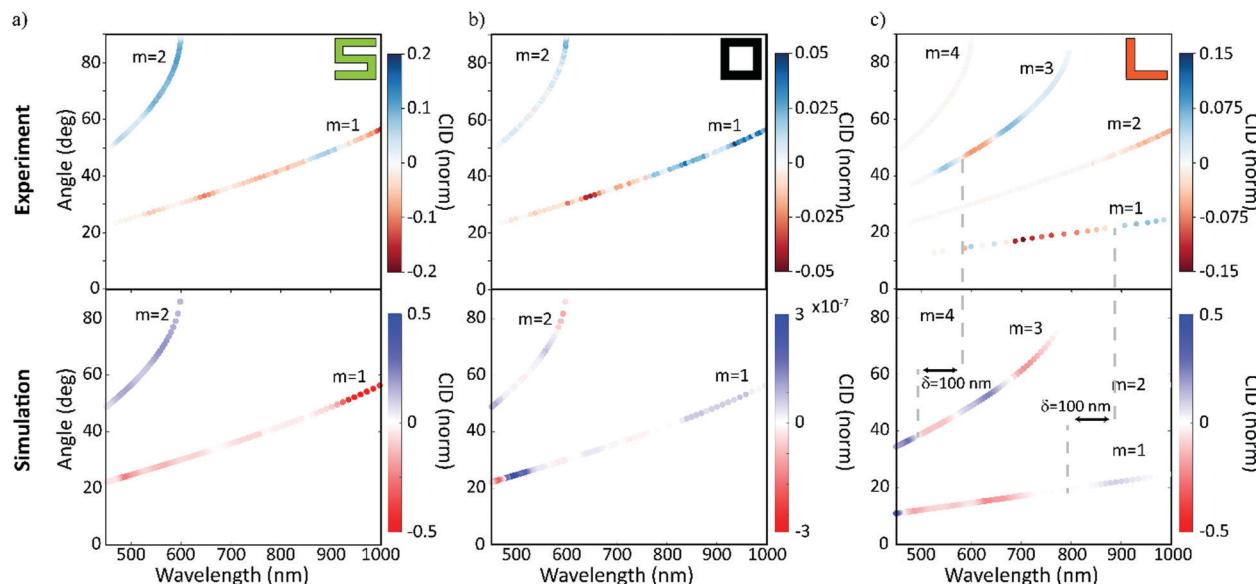
Fig. 3 In diffraction, the response of our racemic nanomaterials is similar to that of the chiral nanomaterials. The results for the circular intensity difference (CID) spectroscopy measurements for the three chiral cases – with chiral (green 'S'), achiral (black 'square-ring') and racemic (orange 'L'). The measured wavelength is shown on the x- and the diffraction angle on the y-axis. The diffracted order beams are numbered, and the color represents the strength and sign of the measured CID signals. The experimental results (top row) are compared with numerical simulations (bottom row) and are in very good agreement. For the racemic case, it should be highlighted that the second and fourth order diffracted beams exhibit no CID, although their intensities are dominant (Fig. 2d). While the chiral and achiral cases agree with our expectations, the racemic case, surprisingly, exhibits a CID comparable to the chiral case.

(see Note 1, ESI†) is employed. In the implementation, the near-field is first decomposed into propagating and non-propagating spatial Fourier modes with their Fourier coefficients being calculated. Then, all the modes are propagated and projected onto an observation plane, so that physical quantities of interests can be obtained, such as electromagnetic fields, power, etc. The reflectance spectrum from the racemic sample is identical under LCP and RCP illumination (see Fig. 4a). This might seem surprising, given that the sample unit cells lack mirror symmetry. However, a careful examination of the sample reveals two additional axes of reflection that do not pass through the rotation centers of the unit cells (see Fig. 4b). Mathematically, these mirroring symmetries, together with the four-fold rotational symmetries, form a D_4 point group. By further considering translational symmetries in the square lattice, the sample actually holds a $p4g$ (wallpaper) group.[36] Especially, due to the axes of reflection, the optical response for LCP and RCP illumination in the experiment can always be transformed into each other by a mirroring operation with respect to the axes of reflection (see Fig. 4d). This transformation leads to, at most, a phase difference and results in identical reflectance spectra for LCP and RCP illumination. The above statements have also been rigorously proven by using an integral equation representation[37–39] in combination with the group representation theory[40] (see Notes 1 and 2, ESI†).

In contrast to the reflectance spectrum, which describes the effect of all the (propagating) Fourier modes, diffraction spectroscopy enables the precise examination of each Fourier mode, thereby revealing the symmetry of the structure. As shown in Fig. 4c, the calculated CID agrees well with our experimental

data (Fig. 3c). The CID can be mathematically attributed to the fact that when evaluating the Fourier coefficients (see Notes 3 and 4, ESI†) for a given direction of diffraction, the phase term $e^{i(k_x x + k_y y)}$ may have a different symmetry than the sample. This observation therefore results in different Fourier coefficients for the LCP and RCP illuminations and further corroborates our argument from the reciprocity point of view.

Lastly, it should be pointed out that the square lattice supports only three wallpaper groups:[36] the $p4$ group, which is generated by the C_4 point group and is exactly the case of the S-shape sample; the $p4m$ group, which is generated by the D_4 point group, whose axes of reflection coincide with the rotational centers of the unit cells and which is exactly the case of the square-ring sample; and the $p4m$ group which is the case of the L-shape sample. By following the same analysis for the L-shape structure, the CID features for the other two cases can be readily derived and are summarized in the Table 1. It is readily seen that reflectance and diffraction circular intensity difference spectroscopy in combination provide us with the powerful capability of identifying the symmetries of a unit cell in the square lattice, without having to analyze the intricate near-field.

Discussion

It is important to distinguish our results from cases of false chirality,[41] whereby chirality in the experiment can be measured instead of chirality in the samples. The Circular Dichroism in the Angular Distribution of Photoelectrons (CDAD) effect was
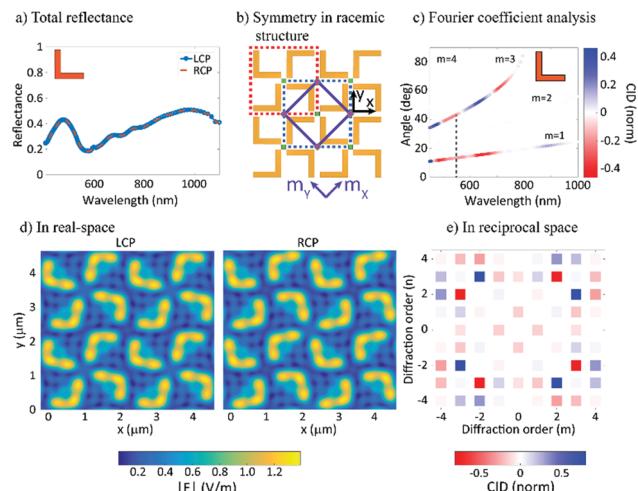
Fig. 4 Fourier modal analysis reveals the effects of chirality on the measured response from the racemic nanomaterials. The total reflectance measured for the racemic sample is shown in (a) for LCP (blue line) and RCP (orange line) – the two cases are identical and thus there is no CID. In (b) the symmetry for the racemic nanostructure is schematically presented. The green squares represent the centers of rotation of the fourth order, while the purple diamonds represent the centers of rotation of the second order. Further, the solid purple lines represent two axes of reflection. The red and green dashed lines delineate the "normal" and "mirror" 4L unit cells, respectively. Lastly, two possible coordinate frames, that is, the x–y coordinate system and the m_x–m_y coordinate system, are marked by the black and purple colors. In (c) the results of the Fourier coefficient analysis are shown and show that there is strong CID in individual diffraction orders, with the first and third diffraction orders showing the strongest CID. The dashed grey line at 554.2 nm indicates the wavelength studied further. In (d) the total electric field magnitude obtained using FDTD simulations at 3 μm above the surface at the indicated wavelength is shown. The result shows the summation of all propagating modes under LCP and RCP illumination respectively. The field maps can be projected into reciprocal space using a Fourier transform, (e). Each point corresponds to the diffraction order beams for the racemic structure for the same wavelength studied in (d). The color-code corresponds to the strength of the normalized CID response. The symmetry is preserved in the diffraction orders and the chiroptical response cancels if summed over all points.

first predicted by Ritchie, in a series of publications.[42–45] CDAD is very different from the CD effect. The CD effect is often small, as it requires contributions from both the electric and the magnetic dipoles, with the latter being usually very small. By contrast, the CDAD effect can originate from electric dipoles only,[46] and as a consequence it was calculated to be much larger than CD, reaching up to 100% of asymmetry.[47] The CDAD effect was first demonstrated experimentally in 1989, by Westphal et al.[48] and the reported results were in good agreement with the theoretical predications.[49–52]

Table 1 Summary of the CID features in the S-shape, L-shape and square-ring-shape samples

	S-shape	L-shape	Square-ring-shape
Reflectance	↙	×	×
Diffraction	↙	↙	×

Importantly, whereas CD requires chirality, CDAD does not.[53] CDAD arises from the interaction of three vectors: the wave vector $\hat{k}$, the surface normal $\hat{n}$ and the direction of photoemission $\hat{p}$. Large dichroic effects are observed as a function of the angle between $\hat{k}$ and $\hat{n}$. Crucially, the effect is only allowed as long as $\hat{k}$, $\hat{n}$ and $\hat{p}$ are not co-planar. In our experimental configuration, where these vectors are co-planar, the CDAD effect is forbidden. Therefore, our results cannot be attributed to CDAD. There is however another case of false chirality, where these vector can be co-planar; this effect is referred to as "pseudo chirality"[54] or "extrinsic chirality".[55]

Pseudo/extrinsic chirality is another case of "chirality of the experiment" and can be observed in achiral samples. It too arises from three vectors, two of which are the same as in CDAD: the wave vector $\hat{k}$ and the surface normal $\hat{n}$. The third vector is the direction of the curvature $\hat{R}$ on the sample. Here again, large dichroic effects are observed as a function of the angle between $\hat{k}$ and $\hat{n}$, and the observed dichroism was found to be proportional to $(1/R)(\hat{R}\cdot\hat{k} \times \hat{n})$.[56] However, in our experiment $\hat{k}$ is parallel to $\hat{n}$, leading to $\hat{k} \times \hat{n} = 0$. Therefore, pseudo/extrinsic chirality is also forbidden and our results cannot be attributed to it.

It is worth mentioning that the idea to separate intrinsic chiral contributions from CDAD by adopting a co-planar experimental configuration has been explored by Attard et al.[57] However, whereas Attard et al. "tentatively" reported asymmetry values of 2% (±1%), our values rise up to 15% and are well-above the noise-level. Attard et al. reported clear asymmetry in the CDAD experimental geometry. This is in agreement with our own calculations presented in Fig. 4e, where the diagonal diffraction beams (non-co-planar configuration) show the largest CID/asymmetry and reverse sign across the plane of incidence.

Methods

Sample fabrication

10 mm × 10 mm × 525 μm single-side polished Si (p-doped)-SiO$_2$ (300 nm) samples are sonicated in successive baths of acetone and IPA (isopropyl alcohol) for 10 minutes, blow dried with compressed ultra-high purity (UHP) N$_2$ and dehydrated on a hotplate (200 °C, 20 min). UV1116-0.5 (Dow Chemical Company) chemically amplified positive-tone photoresist is spin-coated (5,500 rpm, 45 s) and soft-baked on a hotplate (130 °C, 2 min), resulting in a final thickness of ~350 nm. 80 kV electron beam lithography (Nanobeam nB1) is used for the high-resolution patterning, with exposure conditions: pattern optimized area dose between 40–100 μC cm^{-2}, 1.8 nA operating current and a 38 μm main field.[58] A post-exposure bake on a hotplate is performed at 130 °C, 90 s. The samples are developed in MF-CD-26 for 10 s, followed by a de-ionized (DI)-water rinse for 3 min and N$_2$. Physical vapour deposition of Cr/Au (3/30 nm) is performed using a thermal evaporator (Edwards E306) at a base pressure ~1 × 10^{-6} mbar, at an evaporation rate ~0.1 nm s^{-1}. Resist lift-off is carried out in NMP (N-methyl-2-pyrrolidone) at an elevated temperature of 60 °C for 4 hours, followed by fresh NMP

sonication for 2 min, acetone, IPA rinse and UHP N_2 blow dry. For nanoscale surface quality inspection, a Zeiss LEO 1530 VP Scanning Electron Microscope (SEM) operating at 5 keV was used and the SEM micrographs are shown in Fig. 1.

Experimental methods

The experimental setup consisted of a Fianium SC400-2 2 W laser source with a 1064 nm output wavelength and 20 MHz repetition rate and a 5 ps pulse spliced to an in-house fabricated supercontinuum fiber, described in ref. 59 providing a spectrum between 450 and 1050 nm. Two achromatic linear Glan-Laser polarizers were used to control the power output and a remotely controlled quarter-waveplate (QWP) to selectively produce LCP and RCP light. The QWP was chosen for its broad wavelength range as well as its negligible beam deviation (>1 arcsec), which has been tested – shown in Fig. S3 (ESI†). The sample was mounted on an alignment disk, which in turn was mounted on x–y translation stage placed in the center of an optical breadboard. The breadboard was mounted on a remotely controlled rotation stage. The diffracted light from the sample was collected via a 200 µm core diameter multimode fiber (0.22 NA), which was mounted on a fiber launch system, which in turn was mounted on the breadboard at a distance of 15 cm and measured with an Ocean Optics QE Pro spectrometer. The light coupling into the fiber was optimized with a $20\times$ microscope objective with 0.4 NA and 9 mm focal length. The automated setup used a step size of 0.5°; the spectrometer used an integration time of 30 ms and was averaged over 50 scans. The atomic force microscopy micrograph in Fig. 1d was acquired with a Multimode Scanning Probe Microscope (VEECO) operating in contact mode.

Numerical methods

The full-wave simulations were conducted by an FDTD solver, Lumerical.[35] In the simulations, the incident LCP and RCP plane waves are generated by superposing two 90 degrees phased plane waves which are linearly polarized along the x and y directions. All layers in the sample have been take into account. In detail, the Au layer is modeled by the material data from Johnson and Christy,[60] the Cr layer and the Si layer is modeled by the material data from Palik[61] and the reflective index of the SiO_2 layer is assumed to be 1.5. It should be noted that instead of using the nominal thickness, the Au layer is assumed to be 50 nm. Two simulation regions are used. On the one hand, the FDTD simulation region is assumed to have periodic boundary conditions along the x and y directions and perfect matching layers (48 layers) along the z direction. On the other hand, a mesh refinement region including both the Au and Cr layers is imposed to the S-shape structures, the L-shape structures, and the square-rings. The mesh steps along x, y and z directions are 10 nm, 10 nm and 1.5 nm, respectively.

Conclusions

In summary, we have demonstrated for the first time that diffraction circular intensity spectroscopy can be used to measure a strong chiroptical response for racemic nanogratings. We report chiroptical CID values of up to 15%. Our experimental findings are supported by a rigorous Fourier modal analysis. The analysis can identify the chiroptical response of each individual diffracted order beam. The observed chiroptical behavior in the diffracted beams can be seen as a reciprocal to the extrinsic 2D chirality effect. Furthermore, our results enable the distinction of different unit cells (chiral, achiral and racemic) in a square lattice. Our findings allow the tailoring of far-field features of racemic nanostructures to that of molecules, which is key for developing hyper-sensitive chiral molecular characterization.

Conflicts of interest

There are no conflicts to declare.

Acknowledgements

References

1 M. Kuwata-Gonokami, N. Saito, Y. Ino, M. Kauranen, K. Jefimovs, T. Vallius, J. Turunen and Y. Svirko, Phys. Rev. Lett., 2005, 95, 1–4.
2 M. Hentschel, M. Schäferling, X. Duan, H. Giessen and N. Liu, Sci. Adv., 2017, 3, e1602735.
3 R. Mohammadi-Baghaee and J. Rashed-Mohassel, J. Solution Chem., 2016, 45, 1171–1181.
4 S. Yoo and Q.-H. Park, Sci. Rep., 2015, 5, 14463.
5 H. S. Park, T.-T. Kim, H.-D. Kim, K. Kim and B. Min, Nat. Commun., 2014, 5, 5435.
6 A. Canaguier-Durand and C. Genet, Phys. Rev. A: At., Mol., Opt. Phys., 2015, 92, 043823.
7 I. Liberal and N. Engheta, Nat. Photonics, 2017, 11, 149–158.
8 J. B. Pendry, Y. Luo and R. Zhao, Science, 2015, 348, 521–524.
9 Y. Tang and A. E. Cohen, Phys. Rev. Lett., 2010, 104, 163901.
10 Y. Tang and A. E. Cohen, Science, 2011, 332, 333–336.
11 F. Hong, F. Zhang, Y. Liu and H. Yan, Chem. Rev., 2017, 117, 12584–12640.
12 J. T. Collins, C. Kuppe, D. C. Hooper, C. Sibilia, M. Centini and V. K. Valev, Adv. Opt. Mater., 2017, 5, 1700182.
13 V. K. Valev, J. J. Baumberg, C. Sibilia and T. Verbiest, Adv. Mater., 2013, 25, 2517–2534.
14 E. Meggers, Chem. Commun., 2015, 51, 3290–3301.

15 B. Bai, Y. Svirko, J. Turunen and T. Vallius, *Phys. Rev. A: At., Mol., Opt. Phys.*, 2007, **76**, 023811.

16 B. K. Canfield, S. Kujala, K. Laiho, K. Jefimovs, J. Turunen and M. Kauranen, *Opt. Express*, 2006, **14**, 950.

17 J. M. Slocik, A. O. Govorov and R. R. Naik, *Nano Lett.*, 2011, **11**, 701–705.

18 V. K. Valev, N. Smisdom, A. V. Silhanek, B. De Clercq, W. Gillijns, M. Ameloot, V. V. Moshchalkov and T. Verbiest, *Nano Lett.*, 2009, **9**, 3945–3948.

19 K. Konishi, B. Bai, Y. Toya, J. Turunen, Y. P. Svirko and M. Kuwata-Gonokami, *Opt. Lett.*, 2012, **37**, 4446.

20 B. M. Maoz, Y. Chaikin, A. B. Tesler, O. Bar Elli, Z. Fan, A. O. Govorov and G. Markovich, *Nano Lett.*, 2013, **13**, 1203–1209.

21 H. Zhang and A. O. Govorov, *Phys. Rev. B: Condens. Matter Mater. Phys.*, 2013, **87**, 075410.

22 P. Pagliusi, C. Provenzano, A. Mazzulla, L. Giorgini and G. Cipparrone, *Appl. Spectrosc.*, 2008, **62**, 465–468.

23 I. De Leon, M. J. Horton, S. A. Schulz, J. Upham, P. Banzer and R. W. Boyd, *Sci. Rep.*, 2015, **5**, 13034.

24 S. N. Volkov, K. Dolgaleva, R. W. Boyd, K. Jefimovs, J. Turunen, Y. Svirko, B. K. Canfield and M. Kauranen, *Phys. Rev. A: At., Mol., Opt. Phys.*, 2009, **79**, 043819.

25 R. Y. Wang, P. Wang, Y. Liu, W. Zhao, D. Zhai, X. Hong, Y. Ji, X. Wu, F. Wang, D. Zhang, W. Zhang, R. Liu and X. Zhang, *J. Phys. Chem. C*, 2014, **118**, 9690–9695.

26 J. García-Guirado, M. Svedendahl, J. Puigdollers and R. Quidant, *Nano Lett.*, 2018, **18**, 6279–6285.

27 G. K. Larsen, Y. He, W. Ingram and Y. Zhao, *Nano Lett.*, 2013, **13**, 6228–6232.

28 Y. He, K. Lawrence, W. Ingram and Y. Zhao, *ACS Photonics*, 2015, **2**, 1246–1252.

29 M. Schäferling, *Springer Series in Optical Sciences*, Springer International Publishing, Cham, 2017, vol. 205, pp. 87–100.

30 A. Papakostas, A. Potts, D. M. Bagnall, S. L. Prosvirnin, H. J. Coles and N. I. Zheludev, *Phys. Rev. Lett.*, 2003, **90**, 107404.

31 S. L. Prosvirnin and N. I. Zheludev, *Phys. Rev. E: Stat., Nonlinear, Soft Matter Phys.*, 2005, **71**, 037603.

32 A. Potts, W. Zhang and D. M. Bagnall, *Phys. Rev. A: At., Mol., Opt. Phys.*, 2008, **77**, 043816.

33 T. Roy, A. E. Nikolaenko and E. T. F. Rogers, *J. Opt.*, 2013, **15**, 085101.

34 C. Kuppe, C. Williams, J. You, J. T. Collins, S. N. Gordeev, T. D. Wilkinson, N.-C. Panoiu and V. K. Valev, *Adv. Opt. Mater.*, 2018, **1800098**, 1–6.

35 https://www.lumerical.com/.

36 M. S. Dresselhaus, G. Dresselhaus and A. Jorio, *Group Theory: Application to the Physics of Condensed Matter*, Springer Berlin Heidelberg, Berlin, Heidelberg, 2008.

37 X. Zheng, V. K. Valev, N. Verellen, Y. Jeyaram, A. V. Silhanek, V. Metlushko, M. Ameloot, G. A. E. Vandenbosch and V. V. Moshchalkov, *IEEE Photonics J.*, 2012, **4**, 267–282.

38 X. Zheng, V. Volskiy, V. K. Valev, G. A. E. Vandenbosch and V. V. Moshchalkov, *IEEE J. Sel. Top. Quantum Electron.*, 2013, **19**, 4600908.

39 X. Zheng, V. K. Valev, N. Verellen, V. Volskiy, L. O. Herrmann, P. Van Dorpe, J. J. Baumberg, G. A. E. Vandenbosch and V. V. Moshchalkov, *IEEE Photonics J.*, 2014, **6**, 1–13.

40 X. Zheng, N. Verellen, D. Vercruysse, V. Volskiy, P. Van Dorpe, G. A. E. Vandenbosch and V. Moshchalkov, *IEEE Trans. Antennas Propag.*, 2015, **63**, 1589–1602.

41 L. D. Barron, *Molecular Light Scattering and Optical Activity*, Cambridge University Press, Cambridge, 1982.

42 B. Ritchie, *Phys. Rev. A: At., Mol., Opt. Phys.*, 1975, **12**, 567.

43 B. Ritchie, *Phys. Rev. A: At., Mol., Opt. Phys.*, 1976, **13**, 1411.

44 B. Ritchie, *Phys. Rev. A: At., Mol., Opt. Phys.*, 1976, **14**, 359.

45 B. Ritchie, *Phys. Rev. A: At., Mol., Opt. Phys.*, 1976, **14**, 1396.

46 N. A. Cherepkov, *Chem. Phys. Lett.*, 1982, **87**, 344.

47 R. L. Dubs, S. N. Dixit and V. McKoy, *Phys. Rev. Lett.*, 1985, **54**, 1249.

48 C. Westphal, *et al.*, *Phys. Rev. Lett.*, 1989, **63**, 151.

49 C. Westphal, J. Bansmann, M. Getzlaff and G. Schiinhense, *J. Electron Spectrosc. Relat. Phenom.*, 1990, **52**, 613.

50 C. Westphal, J. Bansmann, M. Getzlaff and G. Schiinhense, *Vacuum*, 1990, **41**, 87.

51 G. Schiinhense, *Phys. Ser.*, 1990, **31**, 255.

52 G. Schiinhense, *Vacuum*, 1990, **41**, 506.

53 G. Schöhense, C. Westphal, J. Bansmann, M. Getzlaff, J. Noffke and L. Fritsche, *Surf. Sci.*, 1991, **251**, 132–135.

54 T. Verbiest, M. Kauranen, Y. Van Rompaey and A. Persoons, *Phys. Rev. Lett.*, 1996, **77**, 1456.

55 E. Plum, X.-X. Liu, V. A. Fedotov, Y. Chen, D. P. Tsai and N. I. Zheludev, *Phys. Rev. Lett.*, 2009, **102**, 113902.

56 A. Belardini, M. C. Larciprete, M. Centini, E. Fazio, C. Sibilia, D. Chiappe, C. Martella, A. Toma, M. Giordano and F. Buatier de Mongeot, *Phys. Rev. Lett.*, 2011, **107**, 257401.

57 G. A. Attard, D. Watson, E. A. Seddon, S. M. Cornelius, E. Herrero and J. Feliu, *Phys. Rev. B: Condens. Matter Mater. Phys.*, 2001, **64**, 115408.

58 C. Williams, R. Bartholomew, G. Rughoobur, G. S. D. Gordon, A. J. Flewitt and T. D. Wilkinson, *Nanotechnology*, 2016, **27**, 485301.

59 J. M. Stone and J. C. Knight, *Opt. Express*, 2008, **16**, 2670–2675.

60 P. B. Johnson and R. W. Christy, *Phys. Rev. B: Condens. Matter Mater. Phys.*, 1972, **6**, 4370–4379.

61 E. Palik, *Handbook of Optical Constants of Solids*, Academic Press, 1998.